Quantum Effects in Double Ionization of Argon below the Threshold Intensity

XiaoLei Hao and Jing Chen*
HEDPS, Center for Applied Physics and Technology, Peking University, Beijing 100084, China, and Institute of Applied Physics and Computational Mathematics, P.O. Box 8009, Beijing 100088, China

WeiDong Li
Institute of Theoretical Physics and Department of Physics, Shanxi University, 030006 Taiyuan, China

Bingbing Wang
Laboratory of Optical Physics, Beijing National Laboratory for Condensed Matter Physics, Institute of Physics, Chinese Academy of Sciences, Beijing 100190, China

Xiaodong Wang
College of Physics and Electronic Engineering, Northwest Normal University, Lanzhou, 730070, China

Wilhelm Becker
Max Born Institute for Nonlinear Optics and Short-Pulse Spectroscopy, Max-Born-Strasse 2a, 12489 Berlin, Germany
(Received 28 September 2013; published 20 February 2014)

So far, nonsequential double ionization (NSDI) of atoms can be well understood within a semiclassical or even classical picture. No quantum effect appears to be required to explain the data observed. We theoretically study electron correlation resulting from NSDI of argon in a low-intensity laser field using a quantum-mechanical *S*-matrix theory. We show that quantum interference between the contributions of different intermediate excited states of the singly charged argon ion produces a transition from back-to-back to side-by-side emission with increasing laser intensity, which is in close agreement with the experimental data. For higher intensities, this transition is enhanced by the consequences of depletion of the excited states.

DOI: 10.1103/PhysRevLett.112.073002 PACS numbers: 33.80.Rv, 34.50.Rk

Nonsequential double ionization (NSDI) in strong laser fields has attracted considerable interest during the past two decades (for reviews, see [1,2]) because it is an ideal system to study the multielectron dynamics, especially the field-affected electron-electron correlation. Rescattering has been accepted as the dominant mechanism for NSDI [3,4]. Here, the first electron is released via a tunneling process and then driven back by the laser field into a recollision with the ionic core after the field has reversed its direction. In the resulting inelastic collision, the second electron may be ionized directly (rescattering-impact ionization: RII) or be pumped to an excited state and then be freed by the field (rescattering excitation with subsequent ionization: RESI) at a later time. Intrinsically, NSDI is a quantum process. Yet, thus far, it can be well understood in a classical picture as demonstrated by the great successes of the semiclassical [5–7] or even classical models [8–10] in interpreting the various experimental observations of NSDI. Indeed, for the RII process, no quantum effect has been identified in experiments. The *S*-matrix theory implies essentially the same (classical) rescattering picture of NSDI in the framework of the "quantum trajectory" approach [11] but allows for interferences [12] of different trajectories which, however, have not been observed yet, since, presumably, they are smoothed out by focal averaging, summation over unobserved electron-momentum components, etc.

For NSDI at intensity below the RII threshold intensity (so that the maximal kinetic energy of the returning first-tunneled electron is below the ionization potential of the second electron), it is believed that the RESI process dominates. Recently, several experimental investigations have been performed in this regime and revealed intriguing new features. In particular, the correlated electron distributions for Ar show a transition from side-by-side to back-to-back emission with decreasing laser intensity [13]. In contrast, for Ne, both above and below the intensity threshold, electrons are always preferentially emitted side by side [14]. Theoretically, for Ar a semiclassical model has reproduced the tendency, though not the magnitude, of this transition [15]. Inspection of the trajectories responsible for NSDI showed that back-to-back emission predominantly occurred after multiple recollisions and the Coulomb potential was found to be instrumental for the effect. However, the model did not incorporate excited states of the Ar^+ ion, which is outside the scope of a semiclassical model. More recently, a study at relatively high intensity shows that the correlation distribution of Ar assumes a cross-shape in the limit of a near-single-cycle pulse [16]. A simplified semiclassical model, which includes the decay of the excited state, is able to reproduce the experimental observations [16]. In addition, a rigorous semianalytic study of the RESI process has also been performed based on the strong-field approximation, which shows a strong dependence of the electron momentum distributions on the bound state involved [17,18]. However, all distributions were found to be equally spread over the four quadrants of the momentum-momentum correlation, which is inconsistent with the experimental observations.

In this Letter, we use the S-matrix theory to investigate the correlated electron momentum distribution of the RESI process for Ar below the threshold intensity. Our calculations are based on the velocity-gauge strong-field approximation. The transition amplitude of RESI for channel j is [atomic units (a.u.) $m = \hbar = e = 1$ are used throughout the Letter] [17,18]

$$
\begin{aligned}
M_j(\mathbf{p}_1, \mathbf{p}_2) = & \int_{-\infty}^{\infty} dt \int_{-\infty}^{t} dt' \int_{-\infty}^{t'} dt'' \\
& \times \int d^3\mathbf{k} \langle \psi_{\mathbf{p}_2}^{(V)}(t) | V_2 | \psi_j^{(2)}(t) \rangle \\
& \times \langle \psi_{\mathbf{p}_1}^{(V)}(t') \psi_j^{(2)}(t') | V_{12} | \psi_{\mathbf{k}}^{(V)}(t') \psi_g^{(2)}(t') \rangle \\
& \times \langle \psi_{\mathbf{k}}^{(V)}(t'') | V_1 | \psi_g^{(1)}(t'') \rangle, \qquad (1)
\end{aligned}
$$

where $|\psi_g^{(i)}(t)\rangle$ is the ground state of the ith electron, $|\psi_j^{(2)}(t)\rangle$ the excited state of the second electron, $|\psi_{\mathbf{p}}^{(V)}(t)\rangle$ the Volkov state with asymptotic momentum $\mathbf{p}$, V_1 and V_2 denote the binding potential of the first and second electron, respectively, and V_{12} the interaction between the two electrons. In our calculation V_1, V_2, and V_{12} are given by

$$
V_i = -\frac{Z_{\text{eff}}}{r_i}, \qquad V_{12} = \frac{1}{|\mathbf{r}_1 - \mathbf{r}_2|}, \qquad (2)
$$

where $Z_{\text{eff}} = \sqrt{2I_p}$ is the effective charge and I_p the respective ionization potential. The multiple integrals in Eq. (1) are solved using saddle-point methods (for details see Refs. [17,19]).

The wave functions used in our calculation are obtained numerically based on the method in Ref. [20]. In our calculation, only the states with zero magnetic quantum number are taken into account due to the linear polarization of the laser field. Since there may be more than one channel contributing to double ionization, we have to identify the dominant channels. We have assessed the lowest six ionization channels of Ar^+. Only three of them make the dominant contribution to double ionization in the intensity region of interest. Their configurations are listed in Table I [21].

In Fig. 1, we present the correlated momentum distributions (integrated over the transverse momentum components) for these three channels at different intensities. The figure shows that the shape of the momentum distributions

TABLE I. The configurations of the dominant channels.

Channel	I_p (a.u.)	Configuration
1	0.52	$3s3p^6$
2	0.41	$3s^2 3p^4(^3P)3d$
3	0.18	$3s^2 3p^4(^3P)4d$

varies with channel and intensity. When the ionization channel changes from 1 to 3, the momenta of the two electrons become more and more equal; i.e., the distributions tend to shift from the axes to the diagonals. With increasing intensity, the absolute rates strongly increase. Moreover, we notice that channel 3 is always dominant in the intensity regime considered here.

Next, we calculate the coherent sum of the contributions of different channels, $W_{\text{coh}}(p_{1\|}, p_{2\|}) = \int d^2\mathbf{p}_{1\perp} d^2\mathbf{p}_{2\perp} |\sum_j M_j(\mathbf{p}_1, \mathbf{p}_2)|^2$, where $p_{i\|}$ and $\mathbf{p}_{i\perp}$ denote the components of $\mathbf{p}_i$ parallel and perpendicular to the laser polarization axis. For comparison, we also calculate the incoherent sum of the different channels, $W_{\text{incoh}}(p_{1\|}, p_{2\|}) = \int d^2\mathbf{p}_{1\perp} d^2\mathbf{p}_{2\perp} \sum_j |M_j(\mathbf{p}_1, \mathbf{p}_2)|^2$, in Fig. 2. The momentum distributions of $W_{\text{incoh}}(p_{1\|}, p_{2\|})$ are symmetric with respect to all quadrants, which is a natural consequence of the symmetry of the distributions shown in Fig. 1. However, this is no longer the case for $W_{\text{coh}}(p_{1\|}, p_{2\|})$, which only obeys the particle-exchange symmetry $1 \leftrightarrow 2$. Obviously, this symmetry breaking should be attributed to interference between different channels in the RESI process. More interestingly, for the two lower intensities 4×10^{13} W/cm^2 and 7×10^{13} W/cm^2 the distribution clearly concentrates in the second and fourth quadrants, indicating that the electrons tend to be ejected back to back. In contrast, for the highest intensity (9×10^{13} W/cm^2)

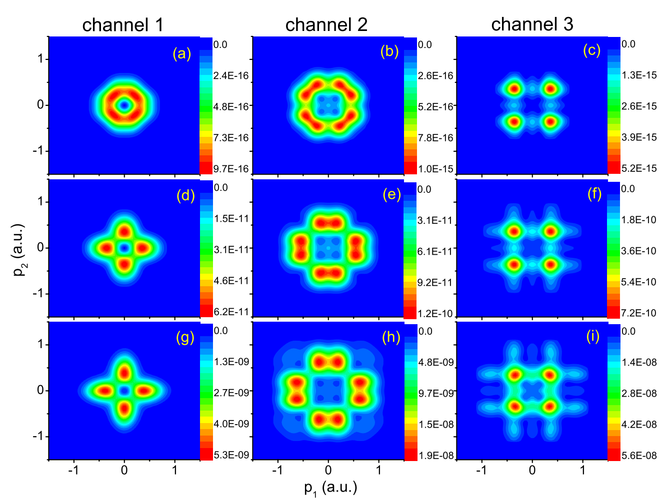

FIG. 1 (color online). Correlated longitudinal momentum distributions corresponding to the three channels of Table I for Ar at different intensities. (a), (b), and (c) 4×10^{13} W/cm^2; (d), (e), and (f) 7×10^{13} W/cm^2; (g), (h), and (i) 9×10^{13} W/cm^2.

TABLE II. The asymmetry parameter with different effects included (TW $= 10^{12}$ W).

I(TW/cm^2)	Interference	Depletion	Interference and depletion
40	−0.204	0.078	−0.319
70	−0.267	0.137	−0.129
90	−0.001	0.404	0.401

the maxima of the distribution in the first and third quadrants exceed those in the second and fourth quadrants [see Fig. 2(f)]. However, integration of the whole distribution shows that the electrons are almost uniformly distributed over the four quadrants (see the entry of −0.001 in the last line of Table II).

This interference effect must be rooted in the phases of the three contributing channels, which are intensity dependent. To see this more clearly, in Fig. 3, we plot the real and imaginary parts of the transition amplitudes [Eq. (1)] of the three channels $j = 1, 2, 3$ for different intensities (for simplicity, we have extracted the phase of channel 2, i.e., we plot the real and imaginary parts of $|M_j|e^{i(\varphi_j-\varphi_2)}$, where φ_j is the phase of the transition amplitude M_j). The momentum of the first electron is fixed while the momentum of the second electron varies along the white dashed line in Fig. 2 (here, only momenta with zero transverse components are considered since the differential ionization rate decreases fast with increasing transverse momentum).

Inspection of Fig. 3 shows a very clean-cut behavior at the lowest intensity: for negative momentum (fourth quadrants in Fig. 2), the three channels interfere constructively both in the real and the imaginary part, while for positive momentum there is marked destructive interference between channels 2 and 3 in the real part. The consequence is the pronounced back-to-back emission that is evident in Fig. 2(b). For the intermediate intensity, we still observe similar though less distinct behavior. For the highest intensity, however, the situation is almost the opposite: the constructive interference of the real parts for positive momentum determines the correlation so that now emission is largely side by side [Fig. 2(f)].

So far, the calculation of Eq. (1) was based on the assumption that once the electron is excited, the population of the excited state can be treated as a constant; i.e., the decay of the excited states due to ionization is ignored. However, this assumption will not be valid when the laser intensity is high or the ionization potential of the excited state is low so that the population of the excited state is quickly depleted due to ionization. Now, we shall modify Eq. (1) to take into account depletion of the excited states. The depletion rate of the excited state is approximately described as $(\gamma_j/2)\sin^2\omega t$, where γ_j is a parameter calculated using a numerical solution of the time-dependent Schrödinger equation [22,23] for each excited state. The resulting transition amplitude can be written as

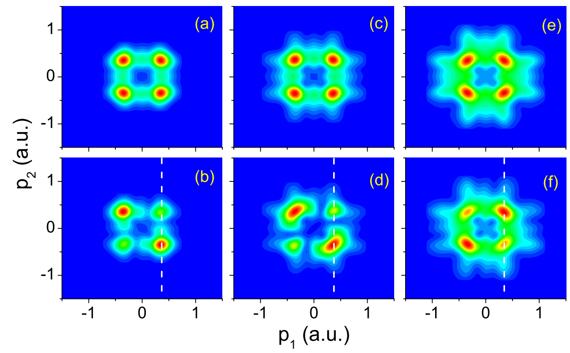

FIG. 2 (color online). Correlated longitudinal momentum distributions without (upper row) and with (lower row) interference between different channels at different intensities. (a) and (b) 4×10^{13} W/cm^2; (c) and (d) 7×10^{13} W/cm^2; (e) and (f) 9×10^{13} W/cm^2. See the text for explanation of the white dashed line. The contour plots have been normalized to the maximal probability in each panel.

$$
\begin{aligned}
M_j(\mathbf{p}_1,\mathbf{p}_2) &= \int_{-\infty}^{\infty} dt \int_{-\infty}^{t} dt' \int_{-\infty}^{t'} dt'' \int d^3\mathbf{k}\, e^{-\int_{t'}^{t}\frac{\gamma_j}{2}\sin^2\omega\tau d\tau} \\
&\quad \times \langle \psi_{\mathbf{p}_1}^{(V)}(t')\psi_j^{(2)}(t')|V_{12}|\psi_{\mathbf{k}}^{(V)}(t')\psi_g^{(2)}(t')\rangle \\
&\quad \times \langle \psi_{\mathbf{p}_2}^{(V)}(t)|V_2|\psi_j^{(2)}(t)\rangle\langle \psi_{\mathbf{k}}^{(V)}(t'')|V_1|\psi_g^{(1)}(t'')\rangle \\
&= \int_{-\infty}^{\infty} dt \int_{-\infty}^{t} dt' \int_{-\infty}^{t'} dt'' \int d^3\mathbf{k} \\
&\quad \times V_{\mathbf{p}_2 j} V_{\mathbf{p}_1 j,\mathbf{k}g} V_{\mathbf{k}g} e^{iS(\mathbf{p}_1,\mathbf{p}_2,\mathbf{k},t,t',t'')}. \qquad (3)
\end{aligned}
$$

Qualitatively, we expect depletion to have two different effects: first, for a state that is a superposition of states with

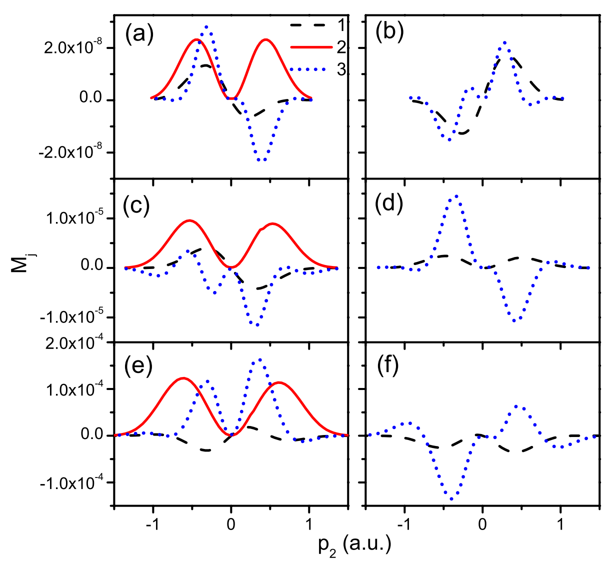

FIG. 3 (color online). Real part (left column) and imaginary part (right column) of the transition amplitude $|M_j|\exp(\varphi_j-\varphi_2)$ vs momentum of the second electron at different intensities. See the text for more details. (a) and (b) 4×10^{13} W/cm^2; (c) and (d) 7×10^{13} W/cm^2; (e) and (f) 9×10^{13} W/cm^2.

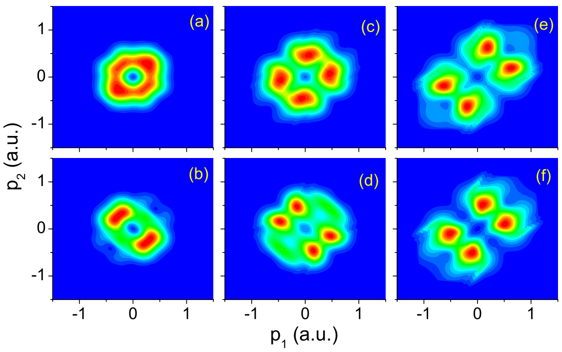

FIG. 4 (color online). Correlated longitudinal momentum distributions without (upper row) and with (lower row) interference between different channels at different intensities with depletion included. (a) and (b) 4×10^{13} W/cm^2; (c) and (d) 7×10^{13} W/cm^2; (e) and (f) 9×10^{13} W/cm^2.

different ionization potentials, an estimate based on the Keldysh ionization rate $R(I_p, U_p) \sim \exp[-(2I_p)^{3/2}/(3\omega\sqrt{U_p})]$ shows that depletion is more important for lower intensity since the difference between ionization rates of different states decreases with increasing intensity; second, depletion will affect the ratio of side-by-side over back-to-back emission since it depends on time.

Figure 4 illustrates the effect of depletion on the incoherent rate, $W_{\text{incoh}}(p_{1\|}, p_{2\|})$ (upper row), and the coherent rate $W_{\text{coh}}(p_{1\|}, p_{2\|})$ (lower row). For a discussion, let us first return to the same results in the absence of depletion (Fig. 2). In this case, we notice that all distributions have a shape much like that of the individual channel 3 [cf. Figs. 1(c), 1(f), and 1(i)]. This is because, according to Table I, channel 3 has by far the lowest ionization potential so that its individual ionization rate is by far the largest. The coherent sum [Fig. 2 (lower row)] differs from its incoherent counterpart [Fig. 2 (upper row)] by the fact that either side-by-side or back-to-back emission becomes dominant owing to interference, as explained above. Now, how does depletion change this picture? Depletion will reduce the contribution of the channel with the lowest ionization potential, which is channel 3, and will be most important for the lowest intensity as argued above. Therefore, the resulting momentum distributions no longer exhibit the basic square shape of Fig. 2, which in turn is a consequence of the dominance of channel 3 [Figs. 1(c), 1(f), and 1(i)], but rather become close to that of channel 1 for the intensity 4×10^{13} W/cm^2 and to a mixture of the contributions of all channels for the intensities of 7×10^{13} and 9×10^{13} W/cm^2.

Both for the incoherent and for the coherent sums in Fig. 4, we observe another tendency: the distributions develop a preponderance of side-by-side over back-to-back emission. The physical reason behind this symmetry breaking due to depletion can be understood as follows: The first electron returns to collide with the second electron most probably near a zero crossing of the laser field. In the next half cycle, if the second electron is ionized before the maximum of the laser field, the two electrons will be ejected side by side. If the ionization happens after the maximum of the laser field, they will move in opposite directions. Since the population of the excited state decreases with time, electrons will more probably be ejected side by side, i.e., more likely be distributed in the first and third quadrants and this asymmetry will become more pronounced when the ionization rate increases.

When both interference and depletion are considered, the electron correlation pattern shows an interesting transition. To show this effect more clearly, we introduce the asymmetry parameter $\alpha = (Y_{1\&3} - Y_{2\&4})/(Y_{1\&3} + Y_{2\&4})$, where $Y_{1\&3}$ and $Y_{2\&4}$ denote the yields of distributions in the first and third quadrants and in the second and fourth quadrants, respectively. In Table II we show the values of the asymmetry parameter when only interference, only depletion, and both are taken into account. We notice that the two effects generally act in opposite directions: interference favors back-to-back emission of the two electrons while depletion supports them going side by side. In addition, interference becomes insignificant at high intensity while depletion continues to increase. It is noteworthy that even though the relative amplitudes of the different channels change when depletion is taken into account, the general picture shown in Fig. 3 does not change according to our calculation. Therefore, the electron correlation undergoes a transition from back-to-back to side-by-side emission when the laser intensity increases from 4×10^{13} to 9×10^{13} W/cm^2, which can also be clearly seen in Figs. 4(b), 4(d), and 4(f). This peculiar transition is in agreement with the experimental observations [13]. We notice that in our results the transition is more pronounced (and, it appears, closer to the data) than in the semiclassical approach [15], which does not account for the excited states of the Ar^+ ion. We also carried out similar calculations for the case of Ne. In contrast to a semiclassical simulation, which predicts a similar transition around 1.2×10^{14} W/cm^2 [14], our calculations indicate that for neon the transition is absent and the electrons are always emitted side by side. This result will be presented elsewhere.

In summary, we have investigated the RESI process in NSDI of Ar at low intensities based on the S-matrix theory. Three dominant channels for double ionization of Ar are identified. Our calculation displays pronounced intensity-dependent interference of the contributions of these channels. This interference causes a concentration of the correlation distribution in the second and fourth quadrants, which becomes weaker with increasing intensity and finally moves to the first and third quadrant. However, the total population of the first and third quadrants (integrated over all contributing momenta) of Fig. 2(f) is almost equal to that of the second and fourth quadrants. On the other hand, depletion of the excited states is also taken into account in our model and this is always found to support a concentration of the distribution in the first and third quadrants, which becomes more pronounced at higher intensity. The two effects compete and, depending on the intensity, counteract each other. The net effect is that the correlation distribution changes from back-to-back emission at low intensity, which is attributed to the interference between different channels of RESI, to side-by-side emission at the highest intensity, which is mainly caused by depletion. Our results qualitatively reproduce the experimental observations of Ref. [13]. Less clean-cut but comparable agreement is obtained within the semiclassical model [15], but the difference is not distinct enough to decide in favor of one or the other model. Much more importantly, however, we have identified a pronounced qualitative quantum interference effect in the NSDI process, which has been elusive so far. This reminds one of the limitations of semiclassical and classical descriptions. Moreover, this kind of quantum interference may also play an important role in NSDI of Ar or He at high intensities where RESI is known to be the dominant mechanism due to the large electron-impact-excitation cross sections of these atoms compared with those of impact ionization [24].

We would like to acknowledge Dr. Xiaojun Liu and Dr. Yunquan Liu for helpful discussions. This work was partially supported by the National Basic Research Program of China (No. 2013CB922201 and No. 2011CB8081002) and NNSFC (No. 10934004, No. 11074155, No. 11274050, No. 11334009, and No. 11374197).

*chen_jing@iapcm.ac.cn

[1] C. Faria and X. Liu, J. Mod. Opt. **58**, 1076 (2011).
[2] W. Becker, X. Liu, P. J. Ho, and J. H. Eberly, Rev. Mod. Phys. **84**, 1011 (2012).
[3] K. J. Schafer, B. Yang, L. F. DiMauro, and K. C. Kulander, Phys. Rev. Lett. **70**, 1599 (1993).
[4] P. B. Corkum, Phys. Rev. Lett. **71**, 1994 (1993).
[5] J. Chen, J. Liu, L. B. Fu, and W. M. Zheng, Phys. Rev. A **63**, 011404(R) (2000).
[6] D. F. Ye, X. Liu, and J. Liu, Phys. Rev. Lett. **101**, 233003 (2008).
[7] X. L. Hao, G. Q. Wang, X. Y. Jia, W. D. Li, J. Liu, and J. Chen, Phys. Rev. A **80**, 023408 (2009).
[8] P. J. Ho, R. Panfili, S. L. Haan, and J. H. Eberly, Phys. Rev. Lett. **94**, 093002 (2005).
[9] P. J. Ho and J. H. Eberly, Phys. Rev. Lett. **97**, 083001 (2006).
[10] F. Mauger, C. Chandre, and T. Uzer, Phys. Rev. Lett. **105**, 083002 (2010).
[11] R. Kopold, W. Becker, H. Rottke, and W. Sandner, Phys. Rev. Lett. **85**, 3781 (2000).
[12] S. V. Popruzhenko, Ph. A. Korneev, S. P. Goreslavski, and W. Becker, Phys. Rev. Lett. **89**, 023001 (2002).
[13] Y. Q. Liu, S. Tschuch, A. Rudenko, M. Dürr, M. Siegel, U. Morgner, R. Moshammer, and J. Ullrich, Phys. Rev. Lett. **101**, 053001 (2008).
[14] Y. Q. Liu *et al.*, Phys. Rev. Lett. **104**, 173002 (2010).
[15] D. F. Ye and J. Liu, Phys. Rev. A **81**, 043402 (2010).
[16] B. Bergues *et al.*, Nat. Commun. **3**, 813 (2012).
[17] T. Shaaran, M. T. Nygren, and C. Figueira de Morisson Faria, Phys. Rev. A **81**, 063413 (2010).
[18] B. B. Wang, Y. C. Guo, J. Chen, Z. C. Yan, and P. M. Fu, Phys. Rev. A **85**, 023402 (2012).
[19] C. Figueira de Morisson Faria, H. Schomerus, X. Liu, and W. Becker, Phys. Rev. A **69**, 043405 (2004).
[20] K. G. Dyall, I. P. Grant, F. A. Parpia, and E. P. Plummer, Comput. Phys. Commun. **55**, 425 (1989).
[21] The other three channels are $3s^2 3p^4 4s$ ($I_p = 0.40$ a.u.), $3s^2 3p^4 4p$ ($I_p = 0.31$ a.u.), and $3s^2 3p^4 5s$ ($I_p = 0.19$ a.u.). The transition probabilities of these channels are at least 2 orders of magnitude smaller.
[22] C. Y. Wu, Y. D. Yang, Y. Q. Liu, Q. H. Gong, M. Wu, X. Liu, X. L. Hao, W. D. Li, X. T. He, and J. Chen, Phys. Rev. Lett. **109**, 043001 (2012).
[23] With the laser field of the form $E(t) = E_0 \sin \omega t$ in our calculation, the formula $(\gamma_j/2)\sin^2 \omega t$ is found to mimic well the time-dependent ionization probability of the excited states obtained in our numerical evolution of the time-dependent Schrödinger equation.
[24] V. L. B. de Jesus, B. Feuerstein, K. Zrost, D. Fischer, A. Rudenko, F. Afaneh, C. D. Schröter, R. Moshammer, and J. Ullrich, J. Phys. B **37**, L161 (2004).